J|A|C|S
ARTICLES
Published on Web 05/12/2006

Origin of Trans-Bent Geometries in Maximally Bonded Transition Metal and Main Group Molecules

Clark R. Landis* and Frank Weinhold

Contribution from the Department of Chemistry, University of Wisconsin−Madison, Madison, Wisconsin 53706

Received February 10, 2006; E-mail: landis@chem.wisc.edu

Abstract: Recent crystallographic data unambiguously demonstrate that neither Ar′GeGeAr′ nor Ar′CrCrAr′ molecules adopt the expected linear (VSEPR-like) geometries. Does the adoption of trans-bent geometries indicate that Ar′MMAr′ molecules are not "maximally bonded" (i.e., bond order of three for M = Ge and five for M = Cr)? We employ theoretical hybrid density functional (B3LYP/6-311++G**) computations and natural bond orbital-based analysis to quantify molecular bond orders and to elucidate the electronic origin of such unintuitive structures. Resonance structures based on quintuple M−M bonding dominate for the transition metal compounds, especially for molybdenum and tungsten. For the main group, M−M bonding consists of three shared electron pairs, except for M = Pb. For both d- and p-block compounds, the M−M bond orders are reflected in torsional barriers, bond−antibond splittings, and heats of hydrogenation in a qualitatively intuitive way. Trans-bent structures arise primarily from hybridization tendencies that yield the strongest σ-bonds. For transition metals, the strong tendency toward sd-hybridization in making covalent bonds naturally results in bent ligand arrangements about the metal. In the p-block, hybridization tendencies favor high p-character, with increasing avidity as one moves down the Group 14 column, and nonlinear structures result. In both the p-block and the d-block, bonding schemes have easily identifiable Lewis-like character but adopt somewhat unconventional orbital interactions. For more common metal−metal multiply bonded compounds such as $[Re_2Cl_8]^{2-}$, the core Lewis-like fragment $[Re_2Cl_4]^{2+}$ is modified by four hypervalent three-center/four-electron additions.

Introduction

The theoretical investigation reported herein was inspired by the recent synthesis and structural characterization of Ar′CrCrAr′ (Ar′ = terphenyl, **1**) by Power and co-workers[1] and their proposal that the observed geometry of this extraordinary transition metal dimer involves the heretofore unknown crystallographic example of direct five-fold metal−metal bonding. Additional motivation is provided by the recent crystallographic characterization[2] of triply bonded Ar′GeGeAr′ (**2**) and the striking observation that maximally bonded RMMR molecules of both the p-block (**2**) and d-block (**1**) adopt planar, trans-bent geometries rather than the linear arrangement seen for acetylene. For RMMR molecules of the p-block, these observations have spawned intense discussion of the nature of the M−M bonding, with widespread disagreement concerning the M−M bond order.[3−7] Similarly, Power's d-block compound **1** raises the following question: Is this the first example of a crystallographically characterized metal−metal quintuple bond? We demonstrate that the electronic structures of such maximally bonded complexes and the origin of trans-bent geometries can be understood by application of surprisingly simple Lewis-

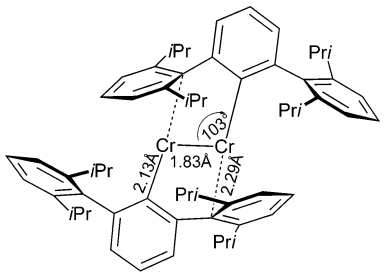

1

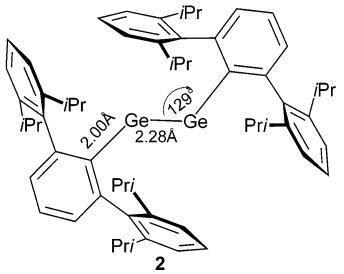

2

(1) Nguyen, T.; Sutton, A. D.; Brynda, S.; Fettinger, J. C.; Long, G. J.; Power, P. P. *Science* **2005**, *310*, 844.
(2) Pu, L. H.; Phillips, A. D.; Richards, A. F.; Stender, M.; Simons, R. S.; Olmstead, M. M.; Power, P. P. *J. Am. Chem. Soc.* **2003**, *125*, 11626.
(3) Power, P. P. In *Group 13 Chemistry, Vol. 1: Fundamental New Developments*; Structure and Bonding 103; Springer: Berlin, 2002; pp 57−84.
(4) Power, P. P. *Chem. Rev.* **1999**, *99*, 3463.
(5) Power, P. P. *Chem. Commun.* **2003**, 2091.
(6) Bouhadir, G.; Bourissou, D. *Chem. Soc. Rev.* **2004**, *33*, 210.
(7) Cowley, A. H. *J. Organomet. Chem.* **2004**, *689*, 3866.

like structures and localized bonds built from directed hybrid orbitals. We conclude that triple-bonded and quintuple-bonded resonance structures play significant roles in **2** and **1**, respectively, and that trans-bent geometries in both the p- and d-block arise from hybridization tendencies that create the strongest σ-bonds.

Bond order is an interpretation, not an observable. Although correlations of measured quantities, such as bond length, with nominal bond orders may be devised for arbitrary collections of compounds, there is no a priori reason for such a relationship. Empirical bond length/bond order correlations appear to follow expected trends for bonds between p-block elements, but extensive compilations of empirical data for d-block elements by Cotton and co-workers[8] led to the conclusion that "bond order and bond length seldom have a truly simple relationship". Throughout this presentation, we use of the term "bond order" in the qualitative sense introduced by Cotton: a measure of "how many electron pairs...play a significant role in holding the atoms together". This definition identifies two critical attributes: the *number* of shared electron pairs and their *significance* in holding a pair of atoms together.[9] Clearly, this view harkens back to the Lewis formulation of chemical bonding, making Lewis-like structures and localized bonding the natural language for interpreting bond order. However, most modern electronic structure computations, such as density functional theory (DFT) and various levels of self-consistent field (SCF) theory, produce delocalized orbitals. Due to the delocalized nature of canonical molecular orbitals (MOs) or Kohn−Sham orbitals and the presence of both constructive and destructive interferences among atomic basis functions, simple counting of MO occupations can give a misleading measure of the number of shared electrons and, thereby, the assigned bond order. Our analyses focus on natural bond orbital (NBO)[10−12] and natural resonance theory (NRT)[13−16] methods applied to densities obtained from hybrid DFT computations. These methods produce simple Lewis-like descriptions with optimal convergence properties for describing localized atomic and bonding regions (see ref 17, p 26) that are largely independent of the basis set or even the sophistication of the computation.

Our presentation begins with a computational examination of the bonding in HMMH models from the p-block. Metrics used to probe the nature and significance of the M−M bond include NBOs, geometries, rotation barriers, heats of hydrogenation, and resonance structure contributions. Analysis of analogues from the Group 6 transition metals follows, using similar methods.

p-Block: Bonding in RMMR Molecules of Group 14

Bonding in maximally bonded elements of the p-block, such as **2**, has received intense scrutiny over the past 10 years.[5−7,18,19] Although there is general agreement that modern electronic structure computations, such as DFT(B3LYP), "reproduce experimentally measured core structural parameters fairly well",[5] the interpretation of the underlying electronic structure and bond order is contentious.[5,20−22] Some of the proposed Lewis-like structures for RMMR compositions of Group 14 elements are shown below; they are labeled according to the assigned formal M−M bond orders.

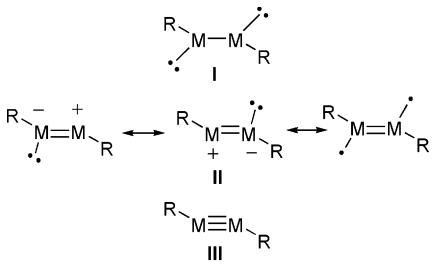

Reluctance to assign a M−M triple bond (**III**) to RMMR, comprising one σ-bond and two π-bonds, originates in their nonlinear geometries. Some bonding formulations seek to account for the trans-bent geometries and maintain the M−M bond order at three. Analysis of electronic structure using localized molecular orbitals (LMOs) led one group of authors[22] to characterize the bonding in $RGaGaR^{2-}$, which is isoelectronic with RGeGeR, as a triple bond (**III**) comprising one π-bond and two σ-like donor−acceptor bonds (π + 2 dative); similar descriptions of Group 14 RMMR compounds have been proposed by Nagase et al.[23] Power[5] notes that a difficulty with this simple model arises if one continues the trans bending to an RMM bond angle of about 90°, as is observed experimentally for RPbPbR.[24] The difficulty is that continued bending lowers the donor overlap, leading to an ultimate evolution into a singly bonded structure such as **I**, but *with a M−M π-bond*, instead of a M−M σ-bond, making the M−M bond. Electronic structures computations,[25] which yield the expected Pb−Pb single bond of σ-type, do not support this and, hence, imply that structure **III** does not capture the essential bonding picture of trans-bent molecules. Klinkhammer[26] used a localized orbital method (NBO) to characterize the bonding in $[RGaGaR]^{2-}$ as triply bonded (**III**), with one σ-bond and one standard π-bond, along with the second "π-bond" having a nonstandard "slipped" character. Two types of valence bond calculations were used

(8) Cotton, F. A. In *Multiple Bonds between Metal Atoms*; Cotton, F. A., Murrillo, C. A., Walton, R. A., Eds.; Springer Science and Business Media: New York, 2005; p 707.
(9) We wish to distinguish "shared" electrons of significant two-center (2c) bonding from "unshared" electrons of primarily one-center (1c) nonbonding character. Paired electrons of the latter type are merely identified as "antiferromagnetically coupled nonbonded (diradical) pairs". Although a sharp distinction between 2c bond and 1c lone-particle character is somewhat arbitrary, the NBO criterion (>5% amplitude at each center for a 2c bond) usually draws this distinction in a chemically reasonable way.
(10) Reed, A. E.; Curtiss, L. A.; Weinhold, F. *Chem. Rev.* **1988**, *88*, 899.
(11) Reed, A. E.; Weinhold, F.; Curtiss, L. A.; Pochatko, D. J. *J. Chem. Phys.* **1986**, *84*, 5687.
(12) Carpenter, J. E.; Weinhold, F. *J. Am. Chem. Soc.* **1988**, *110*, 368.
(13) Glendening, E. D.; Weinhold, F. *J. Comput. Chem.* **1998**, *19*, 593.
(14) Glendening, E. D.; Weinhold, F. *J. Comput. Chem.* **1998**, *19*, 610.
(15) Glendening, E. D.; Badenhoop, J. K.; Weinhold, F. *J. Comput. Chem.* **1998**, *19*, 628.
(16) Feldgus, S.; Landis, C. R.; Glendening, E. D.; Weinhold, F. *J. Comput. Chem.* **2000**, *21*, 411.
(17) Weinhold, F.; Landis, C. R. *Valency and Bonding: A Natural Orbital Donor:Acceptor Perspective*; Cambridge University Press: New York, 2005.
(18) Weidenbruch, M. *Angew. Chem., Int. Ed.* **2005**, *44*, 514.
(19) Weidenbruch, M. *Angew. Chem., Int. Ed.* **2003**, *42*, 2222.
(20) Cotton, F. A.; Cowley, A. H.; Feng, X. J. *J. Am. Chem. Soc.* **1998**, *120*, 1795.
(21) Xie, Y. M.; Schaefer, H. F.; Robinson, G. H. *Chem. Phys. Lett.* **2000**, *317*, 174.
(22) Xie, J. M.; Grev, R. S.; Gu, J. D.; Schaefer, H. F.; Schleyer, P. V.; Su, J. R.; Li, X. W.; Robinson, G. H. *J. Am. Chem. Soc.* **1998**, *120*, 3773.
(23) Nagase, S.; Kobayashi, K.; Takagi, N. *J. Organomet. Chem.* **2000**, *611*, 264.
(24) Pu, L. H.; Twamley, B.; Power, P. P. *J. Am. Chem. Soc.* **2000**, *122*, 3524.
(25) Chen, Y.; Hartmann, M.; Diedenhofen, M.; Frenking, G. *Angew. Chem., Int. Ed.* **2001**, *40*, 2052.
(26) Klinkhammer, K. W. *Angew. Chem., Int. Ed. Engl.* **1997**, *36*, 2320.

by Danovich et al.[27] to investigate the nature of bonding in trans-bent models of HCCH, HSiSiH, and HSiCH. Spin-coupled valence bond calculations for trans-bent HSiSiH yield three largely spin-coupled Si−Si bonds: one of the σ-type, one normal pπ-bond, and one weakened π-like bond that lies in the molecular plane. These authors emphasized that the overall energetics of linear vs bent geometries are governed by the strength of the σ-bonds; indeed, for all three models considered, the σ-bonds are strongest in the bent geometry. Only for acetylene are the π-bonds sufficiently strong to enforce the linear structure.

Canonical molecular orbitals (CMO) for the trans-bent RMMR molecules of the p-block (excluding M = Pb) have been interpreted to indicate one M−M σ-bond, one π-bond, and one nonbonding pair of b_u symmetry that is delocalized over both M atoms and lies in the molecular plane.[5,20,23,28−30] Because just two bonding orbitals are occupied, this model prescribes an M═M double bond, as in **II**, with the nonbonding b_u orbital being equivalent to a resonating lone pair. For the trans-bent silicon, germanium, and tin compounds, the metal s-orbitals make a filled symmetric combination and unfilled, high-energy antisymmetric combination. Upon decreasing the RMM bond angle to 90°, which is primarily observed for Pb, the occupied s-orbitals are increasingly disengaged from bonding, and the symmetric and antisymmetric combinations evolve into two low-lying, nearly degenerate, filled lone pairs as depicted in **I**. Thus, the CMO bonding description of trans-bent RMMR (M = Si, Ge, and Sn) dimers can be represented as shown in structure **II** (whereas the Pb analogue is described as **I** with a Pb−Pb σ-bond). Most critically, the resonance configurations of **II** depict a M═M double bond, with the resonating lone pair being essentially equivalent to the nonbonding b_u CMO. As noted by Power,[5] "it is worrisome" that CMO and LMO bonding models, which are related by unitary transformations, lead to very different M−M bond orders.

More recently, Frenking and co-workers[31] have extended the bonding description so lucidly introduced by Nagase et al.[23] to describe bonding in heavy-atom acetylene-like HMMH models. This description emphasizes the roles played by the $a^4\Sigma^-$ and $X^2\Pi$ states of the HM fragments. Linear geometries result from the coupling of fragments in the $a^4\Sigma^-$ state, whereas bent geometries result from interaction of the $X^2\Pi$ state. This approach generates the "π + 2 dative bonds" description of M−M bonding for the trans-bent geometry. From consideration of all possible donor−acceptor interactions, including donation of H−M bond density into empty orbitals, a lucid picture of the origin of bridged structures, which commonly are the most stable configurations of HMMH models, is devised.

Similar elements arise in describing the electronic structure of trans-bent double bonds (e.g., in R_2MMR_2 molecules with non-carbon elements from Group 14) of the p-block. Pauling[32] and Lappert[33] both described such bent double bonds using resonating lone pairs (**IV**). Another closely related model attributed to Lappert[34] and Malrieu and Trinquier[35] describes the bonding as a double donor−acceptor (paw-paw) interaction between two singlet R_2M fragments (**V**), each bearing an empty p-acceptor orbital and an sp^n-hybridized lone pair. This description emphasizes differences in singlet−triplet gaps as the origin of planar (M = C) and nonplanar (M = Si, Ge, Sn, Pb) geometries. Carter and Goddard[36] showed that bond enthalpies of R_2M═MR_2 double bonds correlate well with singlet−triplet gaps of the R_2M fragments. Trinquier and Malrieu[37] used a valence bond interpretation of CASSCF results to examine contributions from structures **IV** and **V**, taking into consideration also the contribution from the antiferromagnetically coupled π-diradical **VI**. Lappert et al.[34] also introduced a rationalization for bending based on pseudo-Jahn−Teller mixings effected by distortion along the pyramidalization coordinates.

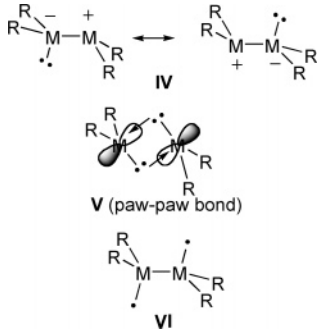

Analyses of multiple bonding in RMMR and R_2MMR_2 compounds by use of electron localization function (ELF),[38,39] atoms in molecules (AIM),[39] and compliance force constant[40] approaches also have been undertaken. Interpretation of the formal bond order using these methods also fails to reach consensus: HGeGeH is described by one set of authors as a triple bond[38] but as bond order of about two by others.[39,40]

Geometries and NBO Analysis of HMMH. In the absence of computations, assignment of the dominant Lewis configuration of trans-bent Ar′MMAr′ (M = Si, Ge, Sn, and Pb) molecules is not clear, nor is the appropriateness of the labels σ and π. DFT computations applied to simple HMMH (M = Si, Ge, Sn, and Pb) models[23,25,31] reproduce the trans-bent structures and approximate M−M bond lengths observed experimentally for the terphenyl compounds, thus indicating that the critical attributes of bonding are captured in these simple models (Table 1).[41] However, it must be noted that trans-bent structures for HMMH models commonly are not the global minimum.[31] Instead, bridged structures generally are more stable. However, terminal RM bonds are consistently observed

(27) Danovich, D.; Ogliaro, F.; Karni, M.; Apeloig, Y.; Cooper, D. L.; Shaik, S. *Angew. Chem., Int. Ed.* **2001**, *40*, 4023.
(28) Bridgeman, A. J.; Ireland, L. R. *Polyhedron* **2001**, *20*, 2841.
(29) Fink, W. H.; Power, P. P.; Allen, T. L. *Inorg. Chem.* **1997**, *36*, 1431.
(30) Allen, T. L.; Fink, W. H.; Power, P. P. *J. Chem. Soc., Dalton Trans.* **2000**, 407.
(31) Lein, M.; Krapp, A.; Frenking, G. *J. Am. Chem. Soc.* **2005**, *127*, 6290.
(32) Pauling, L. *Proc. Natl. Acad. Sci. U.S.A., Phys. Sci.* **1983**, *80*, 3871.
(33) Davidson, P. J.; Harris, D. H.; Lappert, M. F. *J. Chem. Soc., Dalton Trans.* **1976**, 2268.
(34) Goldberg, D. E.; Hitchcock, P. B.; Lappert, M. F.; Thomas, K. M.; Thorne, A. J.; Fjeldberg, T.; Haaland, A.; Schilling, B. E. R. *J. Chem. Soc., Dalton Trans.* **1986**, 2387.
(35) Malrieu, J. P.; Trinquier, G. *J. Am. Chem. Soc.* **1989**, *111*, 5916.
(36) Carter, E. A.; Goddard, W. A. *J. Phys. Chem.* **1986**, *90*, 998.
(37) Trinquier, G.; Malrieu, J. P. *J. Phys. Chem.* **1990**, *94*, 6184.
(38) Grutzmacher, H.; Fassler, T. F. *Chem−Eur. J.* **2000**, *6*, 2317.
(39) Malcolm, N. O. J.; Gillespie, R. J.; Popelier, P. L. A. *J. Chem. Soc., Dalton Trans.* **2002**, 3333.
(40) Pignedoli, C. A.; Curioni, A.; Andreoni, W. *Chemphyschem* **2005**, *6*, 1795.

Table 1. Geometric Quantities and Relative Energies[a] for Linear and Trans-Bent Geometries of HMMH Models of Group 14 Elements, As Computed by DFT(B3LYP) Methods

	trans-bent			linear		E^{rel}
M	R_{MM} (Å)	R_{MH} (Å)	θ_{HMM} (°)	R_{MM} (Å)	R_{MH} (Å)	(kcal/mol)
Si	2.10	1.49	125	1.97	1.46	20.9
Ge	2.26	1.55	124	2.08	1.50	29.5
Sn	2.63	1.73	122	2.40	1.66	38.8
Pb	2.74	1.79	123[b]	3.47	1.85	25.1

[a] $E^{rel} = E^{lin} - E^{bent}$. [b] Not a true minimum on the potential energy surface.

Table 2. NBO Metrics for Trans-Bent HMMH Models That Describe the Metal Natural Charge (Q_M), the Percentage of Total Density Described by the NBO Configuration (ρ_L), and the Compositions (Occupancy, n_{occ}; M Hybridization, h_M; and % Polarization of M, pol) of the σ- and π-like NBOs

			n_{occ}, h_M, pol	
M	Q_M	ρ_L(%)	σ NBO	π NBO
Si	+0.14	97.2	MH: 1.98, $sp^{1.7}$, 43	2.00, p^{∞}, 50
			MM: 1.88, $sp^{1.3}$, 50	1.88, $sp^{4.0}$, 50
Ge	+0.16	96.1	MH: 1.97, $sp^{1.8}$, 45	2.00, p^{∞}, 50
			MM: 1.84, $sp^{1.5}$, 50	1.82, $sp^{3.3}$, 50
Sn	+0.27	94.1	MH: 1.97, $sp^{1.9}$, 37	2.00, p^{∞}, 50
			MM: 1.77, $sp^{1.7}$, 50	1.74, $sp^{4.0}$, 54
Pb	+0.29	93.7	MH: 1.98, sp^{12}, 33	MM: 2.0, sp^{∞}, 50
				1.76, $sp^{0.07}$, lone pair

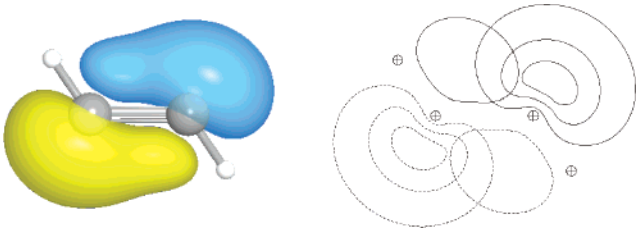

Figure 1. In-plane "slipped bond" (sp-$^{//}\pi$) of HGeGeH as determined by NBO analysis at the B3LYP-optimized geometry.

Table 3. NRT-Computed M−M Bond Orders for Trans-Bent HMMH Models of Group 14 along with Leading Resonance Configuration Populations

M	MM bond order	III	II	I	other
C	2.82	51%	18%	−	30% $H^+ {}^-C{\equiv}CH$
Si[a]	2.79	76%	6%	−	5% $H^- {}^+Si{\equiv}SiH$
Ge[a]	2.51	48%	34%	−	3% $H^- {}^+Ge{\equiv}GeH$
Sn[a]	2.38	35%	44%		5% $H^- {}^+Sn{\equiv}SnH$
Pb[a]	1.97	25%	26%	26%	20% $H^- {}^+Pb{=}PbH$

[a] Many low-population resonance structures are found.

experimentally in isolated RMMR compounds, because only bulky R groups provide the kinetic persistence that allows their synthesis and isolation. This discussion is limited to models with only terminal hydrogens.

NBO analysis (Table 2) identifies three bonds between the Group 14 elements of HMMH. One of these bonds clearly is identifiable as a σ-bond and one as a π-bond with lobes lying above and below the molecular plane. The third bond is π-like, in that it has a single nodal plane but this plane does not contain the internuclear axis. Instead, this π-like orbital is built from two $sp^{3.3}$ hybrids (i.e., hybrids with 77% p-character and 23% s-character) rather than two pure p atomic orbitals (AOs) (see Figure 1). Klinkhammer[26] referred to this bond as a "slipped π-bond"; we introduce the sp-$^{//}\pi$ symbol[42] as a shorthand descriptor. Because the "slipped" sp-$^{//}\pi$-bond achieves lower overlap than a π-bond constructed from pure p-orbitals, there is justification for claiming an effective bond order less than three, even though three pairs of electrons are involved in holding the atoms together.

Lead presents an extreme bonding situation. The trans-bent geometry of HPbPbH is not a true minimum with the B3LYP functional and is included here only for comparison with the geometries of other Group 14 HMMH models. At the trans-bent geometry, NBO analysis yields only a single Pb−Pb bond, testifying to the weakness of the π-interactions. However, the most important feature of this NBO analysis is the poorness of *any* single resonance structure to describe the bonding interactions at this trans-bent geometry; this situation often indicates a very soft potential energy surface at this geometry.

Quantitative Bond Orders from Natural Resonance Theory (NRT). The spirit of "bond order as the number of electron pairs shared in holding two atoms together" is most readily quantified by the population-weighted average of various resonance configurations containing M−M single bonds, double bonds, triple bonds, and so on. In principle, such configurations and their populations can be obtained through multiconfiguration calculations (MC−SCF), but the delocalized nature of each configuration wave function precludes assignment of the bond order to localized pairs of atoms. In contrast, analysis of computed densities via NRT provides a general, localized formulation of bond orders.

As the data of Table 3 indicate, the M−M bond order of Group 14 HMMH models systematically decreases upon moving down the group. Purely on the basis of the number of shared electrons averaged over all resonance structures, it becomes apparent that the bond order lies in the range two to three. Whereas analysis of the electron density using a single NBO configuration forces quantization of the bond order to integral values, use of multiple resonance configurations enables a continuous description that better accommodates expected periodic trends. Note that the Pb−Pb bond order from NRT analysis (bond order = 1.97) is increased relative to that of the best single-configuration NBO structure (bond order = 1), thus illustrating that the optimal single resonance structure description may have either a lower or a higher bond order than the resonance-averaged value.

To this point we have focused on the extent to which electron pairs are shared in holding the two RM fragments of RMMR

(41) All computations reported here were performed with the Jaguar 5.5 electronic structure package and the NBO 5.0 program. Unless otherwise stated, electronic structures were computed using the B3LYP functional with the lacv3p++** basis set, including effective core potentials for elements beyond the second period. Following geometry optimizations, vibrational frequencies were computed to assess the nature of the stationary point. Initial guesses for broken-symmetry calculations were generated using the multiplicity and formal charge features for transition metal fragments that are part of the Jaguar code.

(42) Throughout this work, we use specialized symbols, such as sp-$^{//}\pi$, to indicate unconventional bond orbitals. The first part of the symbol indicates the atomic orbitals used by M to make the bonding hybrid (e.g., s- and p-orbitals), the superscripted symbol evokes a special quality of the orbital (e.g., // represents the tilted orientations of the hybrid with respect to the internuclear axis), and the last symbol represents the most closely related conventional orbital (e.g., π).

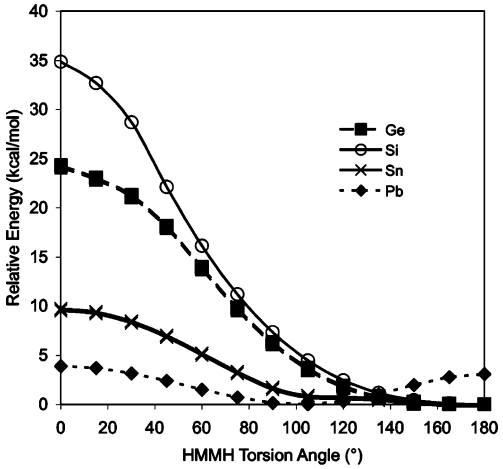

Figure 2. Energy surface for rotation of the main group HMMH central bond with fixed HMM bond angles, as computed by the DFT(B3LYP) method. The M−M bond lengths increase upon rotating from 180° to 0° (Si, 2.105 to 2.572 Å; Ge, 2.259 to 2.565 Å; Sn, 2.634 to 3.165 Å).

together. Now we turn to various measures for gauging the strengths of these interactions.

Rotation about the HM−MH Bond. The existence of trans-bent geometries implies that key orbital interactions are weakened upon rotation about the M−M bond. By performing rigid rotations about the HM−MH bond, where rigidity refers to fixing the HMM angles at the values of the trans-bent minimum while optimizing all bond lengths, some measure of the off-axial orbital interaction strength is gauged. Energy surfaces for rigid rotation about p-block HM−MH bonds show continuous destabilization upon proceeding from 180° to 0° torsion angle (Figure 2). This shape is primarily due to loss of π-like overlaps involving "slipped" sp-$^{//}\pi$-bonds and increased HM bond pair repulsions. The balance among different limiting Lewis structures, such as **I** vs **II** vs **III**, is particularly delicate and depends on the nature of M. For example, with M = Si, the M−M bonding at both the 0° and 180° extrema consists of one σ-bond, one π-bond, and one "slipped" sp-$^{//}\pi$-bond. Weakened sp-$^{//}\pi$ overlap is the primary difference between a cis-bent maximum and a trans-bent minimum (vide infra). In contrast, when M = Ge and Sn, rotation to the 0° HMMH torsion angle results in dramatic lengthening of the M−M bond (0.3 and 0.2 Å, respectively), and NBO analysis clearly indicates the singly bonded structure **III** as the best descriptor. Thus, much of the difficulty in ascribing a definitive bond order to RMMR molecules of the p-block occurs as the result of weak interactions that yield multiple states of similar energy.

With HPbPb bond angles of 123°, the lead dimer is on a soft, high-energy portion of the potential energy surface. A slight minimum near 100° results from increased donation of electron density from a Pb−H bond into an empty p-orbital on the adjacent Pb center.[31]

Bond−Antibond Splittings. As two orbitals on different centers interact to form a bond, the splitting between the symmetric (bonding) and antisymmetric (antibonding) orbitals increases. Thus, the energy difference, or splitting, between the localized bonding and antibonding orbitals provides a measure of the strength of the bonding interactions.[43] Such splittings for HMMH models in the trans-bent geometry (Table 4) reveal the expected trends: σ-bonds are stronger than π-bonds which, in turn, are stronger than slipped sp-$^{//}\pi$-bonds. Furthermore, all

Table 4. Energy Differences (kcal/mol) between Bonding and Antibonding NBOs of Group 14 Trans-Bent HMMH Models

NBO	Si	Ge	Sn	Pb
M−M sp-π	95	59	42	−
M−M p-π	107	89	71	67
M−H sp-σ	414	404	336	298
M−M sp-σ	453	519	376	−

Table 5. Energies (kcal/mol) of Hydrogenation Reactions for Main Group M−M Bonds According to $H_nMMH_n + H_2 \rightarrow H_{n+1}MMH_{n+1}$ (or MH_4 or MH_6)

M	$n = 1$	$n = 2$	$n = 3$
C	−49.8	−38.5	−19.9
Si	−49.6	−51.4	−6.5
Ge	−36.6	−40.5	−3.0
Sn	−24.3	−27.8	4.1

bonding interactions become weaker as one moves down Group 14. Note that the single Pb−Pb bond is of the π-type at the trans-bent geometry. As mentioned previously, rotation about the HSi−SiH bond particularly weakens the slipped sp-$^{//}\pi$-bond while maintaining the other σ- and π-bonding interactions. At a HSi−SiH torsion angle of 0°, the bond−antibond splitting of the slipped sp-$^{//}\pi$-bond is lowered by 40% (to 55 kcal/mol) relative to that of the trans orientation, although the other bond splittings are affected by less than 4%.

Heats of Hydrogenation. Energies of hydrogenation provide another, indirect measure of bond character and relative bond strengths, although interpretation is clouded by differing hybridizations and bond enthalpies of the H−M bonds as the degree of saturation increases. In Table 5, the computed heats for stepwise hydrogenation of HMMH molecules of the p-block are presented. Hydrogenation of π-like bonds (i.e., $n = 1$ and 2) releases substantially more energy than hydrogenation of the M−M σ-bond as expected on the basis of the relative π- vs σ-bond strength. The absolute magnitude of energy release decreases going down the Group 14 column, reflecting the general trend of weakened bonds for the heavier group elements. Note that for M = C, the first hydrogenation is substantially more exothermic than the second; this order is reversed for the heavier Group 14 members.

Origin of Linear vs Trans-Bent Structures. Why do the HMMH models of the heavier p-block elements not form two normal p-π-bonds with linear structures? Three general principles apply: (1) the strongest bonding interactions, σ-bonds, have the greatest impact on orbital directionality and molecular shape (ref 17, pp 107 and 27); (2) there is an increasing tendency for σ-bonding hybrids to have p-character as the mass of M increases; and (3) the remaining bond-forming orbitals must maintain orthogonality with one another and the σ-bonding hybrids. The tendency toward lower s-character (or higher p-character) in M−H and M−M bonds as one moves down the Group 14 column is manifested even in the $X^2\Pi$ state of the HM fragments: the percent s-character of the hybrid orbital making M−H bonds follows the trend C (14.5%) > Si (9.3%) > Ge (7.7%) > Sn (6.9%) > Pb (5.4%). Hybridization tendencies originate in the valence s- and p-AO radial distribu-

(43) Note that the energies of antibonding NBOs, like those of virtual MOs, have problematic physical significance due to the curious "self-repulsion" feature of SCF theory. Nevertheless, these antibond energies are the correct quantities for evaluating perturbative "splittings" of the type considered here.

tions, which are well-matched for carbon but disparate for lead, and bond polarities (Bent's rule), which change directionality on moving from carbon to lead.

If HMMH models of the heavier Group 14 elements were to adopt the linear geometry of acetylene, the H−M and M−M σ-bonds would be forced, via orthogonality constraints, to adopt average sp^1 hybridization and 50% s-character. Lower total energy results from σ-bonds having less s-character (ca. $sp^{1.9}$ or 35% s-character). In keeping with these hybridization tendencies, the HMM bond angles are significantly less than 180°. Although the trans-bent geometry enables one pure p-π-bond perpendicular to the molecular plane, orthogonality constraints force construction of the in-plane sp-$^{//}\pi$-bond from $sp^{3.3}$ hybrids, yielding the "slipped" structure of the sp-$^{//}\pi$-bond orbital. Only for carbon is the three-fold combination of lowered tendency of p-character in σ-bonds, high π-bond strength, and low $X^2\Pi \rightarrow a^4\Sigma^-$ excitation energy for the M−H fragment sufficient to favor the linear geometry; this constitutes a manifestation of the usual "first-element distinctness" (ref 17, p 717) within a vertical column of the periodic table.

The bond lengths in trans-bent HMMH models of the p-block are longer than those in the linear arrangements, despite the routinely higher energy of the latter (see Table 1). For the p-block molecules, such a trend is expected because the linear molecules necessarily have higher s-character within the σ-bonds due to the symmetry-enforced sp^1 hybridization versus $\sim sp^2$ σ-bond hybridization for the trans-bent structures. As a result, the M−H bonds also are shorter for the linear geometry.

Similar considerations lead to the nonplanar R_2MMR_2 molecules of the heavier p-block elements. Unlike ethylene, a "slipped" sp-$^{//}\pi$-bond constitutes the sole "π-like bond" of the non-carbon R_2MMR_2 molecules so as to retain high p-character in the σ-bonds.

For the model dianion, $[HGaGaH]^{2-}$, in the gas phase we find bonding descriptors that clearly are similar to those of isostructural and isoelectronic HGeGeH. Thus, the Ga−Ga bonding comprises one sp-σ-bond, one p-π-bond, and one slipped sp-$^{//}\pi$-bond with a net bond order of ca. 2.5. Directionality is weakened for the dianion; thus, the rigid-rotation barrier (19.2 kcal/mol) and the bond−antibond splittings (e.g., 37.1 kcal/mol sp-π gap) for $[HGaGaH]^{2-}$ are lower than those for HGeGeH. Although the experimentally characterized Ga−Ga dianions have large aryl groups in place of the H atoms and counterions, one can safely describe these controversial dimers with the simple, localized components used for maximally bonded Group 14 dimers.

d-Block: Bonding in RMMR Molecules (M = Cr, Mo, W) of Group 6

Let us begin by summarizing the principles of localized bonding in the d-block (ref 17, p 574, and refs 44−49) before examining the origins of trans-bent structures. We have shown that covalent bonds at transition metal centers form through the

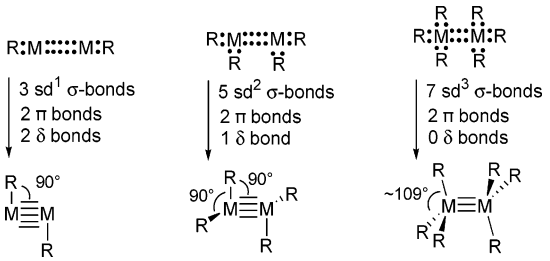

Figure 3. Lewis-like structures, hybridizations, and approximate molecular shapes for quintuple, quadruple, and triple bonding of Group 6 transition metal complexes.

hybridization of valence s- and d-orbitals (e.g., the 4s- and 3d-orbitals of the first transition series). Because this valence space has six total orbitals, saturation occurs at six electron pairs. Therefore, simple Lewis-like structures for transition metal complexes require six placeholders for electron pairs.[50] Hybridization at transition metal centers has the following tendencies: (1) lone pairs tend to favor pure d-character (unlike the p-block elements, which favor high s-character); (2) σ-bonds adopt sd^{n-1} hybridization, where n is the total number of bonds formed at that center; and (3) π- and δ-bonds generally have pure d-character. Notable simple examples include WH_6 (six bonds with sd^5 hybridization) and PtH_2 (four pure d lone pairs and two sd^1 hybrids). As with sp^n hybrids of the p-block, each sd^n hybridization associates with specific preferred angles: sd^1 (90°), sd^2 (90°), sd^3 (71°, 109°), sd^4 (66°, 114°), and sd^5 (63°, 117°). From such relationships, one readily derives the molecular shape of PtH_2 as bent with a bond angle of 90°. For WH_6, four structures place six hydrogens such that all H−W−H bond angles are either 63° or 117°. Two of these structures have C_{3v} point group symmetry, and two have C_{5v} symmetry. Predictions based on localized bonding principles are consistent with the results of ab initio computations for these two examples and many other transition metal complexes. Prediction of the C_{3v} structure of WMe_6 by use of molecular mechanics algorithms based on these simple concepts preceded its crystallographic characterization[51] with remarkable fidelity.

Consider the construction of Lewis-like structures for R_n-MMR_n molecules with M = Cr, Mo, or W, R = methyl or hydride, and $n = 1-3$. Six active orbitals and 12 electrons about the metal center lead to the Lewis-like structures and hybridizations shown in Figure 3. For $n = 1$ and $n = 2$, idealized angles between σ-bonds are ca. 90°, leading to distinctly nonplanar geometries; bonding is completed by the addition of π- and δ-bonds. For $n = 1$, maximal M−M bonding prescribes a quintuple bond; for $n = 2$, a quadruple bond results. With $n = 3$, σ-bond hybrid orbitals of approximately sd^3 hybridization give rise to cylindrical (C_3) symmetry about the triply bonded M−M axis.

More subtle features of the bonding arise from hybrid orbital orthogonality considerations (ref 17, p 378). For the example of sd^1 hybridization, as occurs in RMMR, the construction of *equivalent*, *maximum strength*, *orthogonal* hybrids requires mixing of *two* d-orbitals with an s-orbital of M. The result is two $sd^{1.5}$ hybrids (eqs 1 and 2) that make the H−M and M−M σ-bonds and one sd^4 hybrid (eq 3) that lacks the concentration

(44) Landis, C. R.; Cleveland, T.; Firman, T. K. *J. Am. Chem. Soc.* **1995**, *117*, 1859.
(45) Landis, C. R.; Cleveland, T.; Firman, T. K. *Science* **1996**, *272*, 179.
(46) Firman, T. K.; Landis, C. R. *J. Am. Chem. Soc.* **2001**, *123*, 11728.
(47) Landis, C. R.; Cleveland, T.; Firman, T. K. *J. Am. Chem. Soc.* **1998**, *120*, 2641.
(48) Landis, C. R.; Firman, T. K.; Root, D. M.; Cleveland, T. *J. Am. Chem. Soc.* **1998**, *120*, 1842.
(49) Weinhold, F.; Landis, C. R. *Chem. Educ. Res. Pract. Eur.* **2001**, *2*, 91.
(50) The normal-valent 12e Lewis-like species will often be modified by coordinate additions, as described later in this section.
(51) Pfennig, V.; Seppelt, K. *Science* **1996**, *271*, 626.

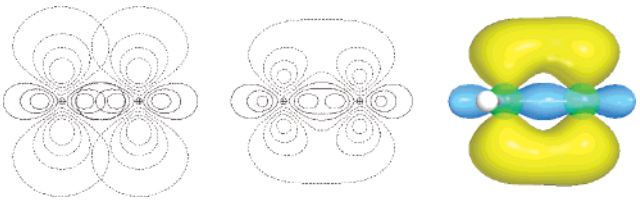

Figure 4. Contour and surface plots for the HWWH side-on d-bond (sd-$^{\pi}\delta$) hybrid orbitals (left, contour plot only) and the sd-$^{\pi}\delta$-bond orbital viewed along the molecular plane (the white sphere shown on the surface plot represents the H atom that lies above the plane of the paper in the trans-bent geometry).

of angular amplitude needed for making a good σ-bond.

$$\text{“sd}^1\text{” hybrid(1)} = 0.632\text{s} + 0.790\text{d}_{z^2} - 0.112\text{d}_{x^2-y^2} \quad (1)$$

$$\text{“sd}^1\text{” hybrid(2)} = 0.632\text{s} - 0.451\text{d}_{z^2} + 0.627\text{d}_{x^2-y^2} \quad (2)$$

$$\text{“sd}^1\text{” hybrid(3)} = 0.447\text{s} - 0.450\text{d}_{z^2} + 0.775\text{d}_{x^2-y^2} \quad (3)$$

These three orbitals are displayed in quotes (“sd^1”) because they do not have *precise* sd^1 composition, although they do have the greatest possible similarity (in a least-squares sense) to two equivalent but non-orthogonal sd^1 hybrids with maximal angular amplitude along the internuclear axis. Three remaining d AOs on each metal center are unhybridized and spatially oriented to make two d-π-bonds and one d-δ-bond.

Where is the fifth bond in the M−M quintuple bond? This bond arises from edge-on overlap of the final “sd^1” (sd^4) hybrids (eq 3), each oriented perpendicular to the internuclear axis (Figure 4). Although such an NBO formed from d-based hybrids might be identified as a “δ-bond”, it has neither the nodal planes nor the symmetry characteristics of the Δ irreducible representation in the $D_{\infty h}$ point group (the proper symmetry label is Σ_g^+). However, like a true δ-bond, this NBO has rather weak overlap, a small energy difference between bonding and antibonding orbitals, and two distinct nodal *surfaces* when viewed along the internuclear M−M axis. Indeed, viewed along the M−M bond, this NBO resembles a d_{z^2} AO with a somewhat amplified “horse collar”. However, compared with an authentic δ-orbital, which is invariant under a 90° ($\pi/2$, C_4) rotation, the NBO shown in Figure 4 is invariant under 180° (π, C_2) rotation. We therefore propose the pragmatic descriptor, “side-on *d*-bond”, and the symbol “sd-$^{\pi}\delta$” for this distinctive type of orbital, to signify its somewhat impure diatomic symmetry character but energetic similarity to δ-type orbitals.

Aside from this interesting technicality, we may summarize by saying that simple hybridization and Lewis-like structure concepts predict that RMMR (M = Cr, Mo, W) molecules in their closed shell configurations should adopt a bent geometry with approximately 90° R−M−M bond angles and M−M quintuple bonds (ref 17, p 415, and ref 49).

As revealed by numerous examinations of simple transition metal diatomics,[52−65] metal−metal bonded dimers have complicated electronic structures due to contributions from multiple, nearly degenerate configurations. Because M−M bonds are relatively weak and intraatomic exchange energies large, the overall electronic structure of the diamagnetic ground state represents a balance between extremes, consisting of one with normal shared electron pair bonds (i.e., closed-shell, maximally bonded limit) and one consisting of two antiferromagnetically coupled atoms, each having localized spin densities that maximize atomic exchange stabilization. In fact, the diatomic Cr_2, most closely related to Power's chromium dimer, **1**, represents perhaps the greatest challenge to electronic structure characterization among all simple diatomic molecules. Both multireference CI and DFT computations reveal multiconfigurational character in Cr_2. On the basis of the results of CASPT2 computations, Roos[55] characterizes Cr_2 as highly multiconfigurational; the sextuply bonded, closed-shell configuration contributes about 45% to the total electronic structure. Because DFT computations are intrinsically monodeterminantal, contributions of multiple configurations are detected indirectly. As shown by numerous DFT studies[52,56] of Cr_2, the closed-shell singlet configuration yields a bond that is too short (by ca. 0.03 Å) and too weak (conversion to two chromium atoms in their ground state is exothermic) to account for experimental data (1.68 Å bond length; 1.54 eV/mol bond dissociation energy). However, broken-symmetry, unrestricted DFT computations result in much lower total energies[52,56] (by ca. 100 kcal/mol) and stronger bonds but contaminate the wave function with higher spin character. Significant energy lowering of a singlet state upon symmetry-breaking indicates multiradical character in the wave function. State-mixing that introduces spin contamination permits the spatial wave function to better approximate the density distribution of the true multideterminantal density but at the expense of less realistically describing the net spin. Extensive DFT computations[52,56] have established that, under favorable conditions, such broken-symmetry computations can reproduce the experimental bond energy, bond length, and energy vs distance profile with impressive accuracy. However, the behavior of different functionals is capricious, with some functionals (particularly hybrid functionals) yielding very long Cr−Cr bonds (ca. 2.3 Å). NBO analysis of broken-symmetry DFT(BLYP) computations, which match experimental metrics well, describes the bonding of Cr_2 as a quadruple bond with significant local spin character (±2.7 spin density on each atom).

Geometries and NBO Analysis of Group 6 HMMH Models. The difficulty of obtaining an adequate electronic structure for chromium dimer dictates caution in the analysis of Group 6 RMMR molecules. We have used DFT computations with both hybrid (B3LYP) and non-hybrid (BLYP) functionals to examine RMMR molecules with M = Cr, Mo, and W and a variety of R groups. In this presentation, we limit ourselves to

(52) Gutsev, G. L.; Bauschlicher, C. W. *J. Phys. Chem. A* **2003**, *107*, 4755.
(53) Gutsev, G. L.; Mochena, M. D.; Jena, P.; Bauschlicher, C. W.; Partridge, H. *J. Chem. Phys.* **2004**, *121*, 6785.
(54) Andersson, K.; Roos, B. O.; Malmqvist, P. A.; Widmark, P. O. *Chem. Phys. Lett.* **1994**, *230*, 391.
(55) Roos, B. O. *Collect. Czech. Chem. Commun.* **2003**, *68*, 265.
(56) Schultz, N. E.; Zhao, Y.; Truhlar, D. G. *J. Phys. Chem. A* **2005**, *109*, 4388.
(57) Barden, C. J.; Rienstra-Kiracofe, J. C.; Schaefer, H. F. *J. Chem. Phys.* **2000**, *113*, 690.
(58) Dachsel, H.; Harrison, R. J.; Dixon, D. A. *J. Phys. Chem. A* **1999**, *103*, 152.
(59) Celani, P.; Stoll, H.; Werner, H. J.; Knowles, P. J. *Mol. Phys.* **2004**, *102*, 2369.
(60) Boudreaux, E. A.; Baxter, E. *Int. J. Quantum Chem.* **2004**, *100*, 1170.
(61) Boudreaux, E. A.; Baxter, E. *Int. J. Quantum Chem.* **2001**, *85*, 509.
(62) Boudreaux, E. A.; Baxter, E. *Int. J. Quantum Chem.* **2005**, *102*, 866.
(63) Goodgame, M. M.; Goddard, W. A. *Phys. Rev. Lett.* **1985**, *54*, 661.
(64) Goodgame, M. M.; Goddard, W. A. *Phys. Rev. Lett.* **1982**, *48*, 135.
(65) Goodgame, M. M.; Goddard, W. A. *J. Phys. Chem.* **1981**, *85*, 215.

Table 6. Geometric Quantities and Relative Energies[a] for Linear and Trans-Bent Geometries of HMMH Models of Group 6 Elements, As Computed by Restricted DFT(B3LYP) Methods

	trans-bent			linear		E^{rel}
M	R_{MM} (Å)	R_{MH} (Å)	θ_{HMM} (°)	R_{MM} (Å)	R_{MH} (Å)	(kcal/mol)
Cr	1.64	1.64	88	1.58	1.67	7.5
Mo	2.03	1.72	91	1.94	1.78	21.1
W	2.10	1.71	93	2.00	1.73	30.9

[a] $E^{rel} = E^{lin} - E^{bent}$.

R = H (Table 6). Energy minimizations of closed-shell configurations routinely optimize to trans-bent structures with approximately 90° H−M−M bond angles, thus resembling the crystallographically characterized terphenyl chromium dimer, **1**. However, the computed Cr−Cr distances (1.64−1.67 Å) are substantially shorter than the experimental distance (1.83 Å). Whether at the energy-minimized distance or the experimental distance, NBO analysis of the closed-shell configuration robustly describes a Cr−Cr quintuple bond.

Broken-symmetry computations indicate significant multiconfigurational character for HCrCrH but little for HMoMoH and HWWH. For the chromium complex, breaking symmetry by using a spin-polarized initial guess leads to modest energy lowering (about one-third the energy lowering obtained by broken symmetry for Cr_2). At short Cr−Cr distances (ca. 1.65 Å), NBO analysis of the broken-symmetry wave function indicates a quintuple bond with modest spin polarization. However, at the experimental separation of 1.83 Å, the best *single-resonance* structure obtained by NBO analysis is a quadruple bond with one α spin and one β spin localized on the Cr atoms. However, we will show that this is not the dominant resonance structure in a multiple-resonance structure analysis. For the Mo and W complexes, broken-symmetry calculations yield little energy lowering or change in the nature of the electron-density distribution. We focus primarily on closed-shell computational results, with the caveat that the absence of multiconfigurational character affects some values, especially for the chromium dimer.

Ab initio DFT computations for closed-shell configurations of HMMH models provide sterling verification of predictions based on localized bond concepts (Table 7). For example, the trans-bent geometry with 90° HMM bond angles appears to be the global minimum for all Group 6 HMMH models in their diamagnetic ground states (which are the lowest energy spin states). This structural motif is precisely that found in Power's recent chromium dimer, **1**. NBO analysis of the electron densities indicates six covalent bonds at each metal center, comprising one M−H σ-bond with ~sd^1 hybridization, one M−M σ-bond with ~sd^1 hybridization, two M−M d-π-bonds, one true M−M d-δ-bond, and one M−M side-on d-bond (sd-$^{\pi}\delta$), as illustrated in Figure 5.

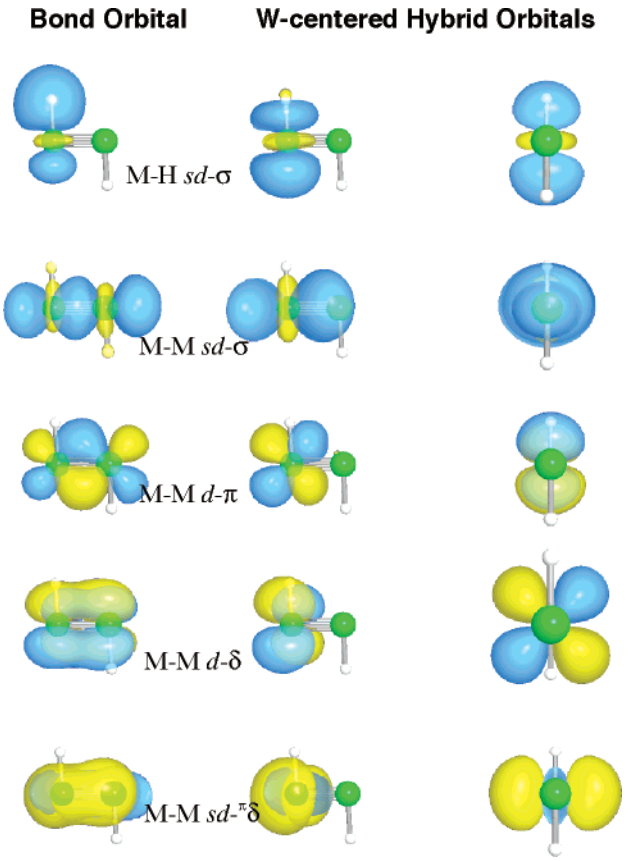

Figure 5. Natural bond orbitals (NBOs, left column) and W-centered natural hybrid orbitals (NHOs) shown both perpendicular to (center column) and along (right column) the W−W axis for trans-bent HWWH. Depicted orbitals include sd-hybridized M−H (top row) and M−M (second row) σ-bonds, one M−M d-δ-bond (third row), one of the two equivalent M−M d-π-bonds (fourth row), and the M−M side-on d-bond (sd-$^{\pi}\delta$) (fifth row).

In the following sections, we address the nature of trans-bent bonds by examining barriers to rotation about the M−M bond, changes in electronic structure associated with distortion to linear geometries, computed heats of hydrogenation, and the bond−antibond energy gaps for various orbital interactions, parallel to the previous discussion of p-block bonding.

Quantitative Bond Orders from Natural Resonance Theory (NRT). As discussed previously, a robust measure of the number of electron pairs shared between two atoms is provided by the populations of various limiting resonance forms. For Group 6

Table 7. NBO Metrics for Trans-Bent HMMH Molecules That Describe the Metal Natural Charge (Q_M), the Percentage of Total Density Described by the NBO Configuration (ρ_L), and the Compositions (Occupancy, n_{occ}; M Hybridization, h_M; and % Polarization of M, pol) of the σ-, π-, and δ-like NBOs

			n_{occ}, h_M, pol		
M	Q_M	ρ_L(%)	σ NBO	π NBO	δ NBO
Cr	+0.38	97.4	MH: 1.89, $sd^{1.5}$, 32	2.00, sd^{∞}, 50	d-δ: 2.00, sd^{∞}, 49
			MM: 1.92, $sd^{2.3}$, 50	1.97, sd^{∞}, 50	sd-$^{\pi}\delta$: 1.99, $sd^{4.7}$, 50
Mo	+0.26	98.4	MH: 1.94, $sd^{1.5}$, 37	2.00, sd^{∞}, 50	d-δ: 2.00, sd^{∞}, 49
			MM: 1.97, $sd^{1.4}$, 50	1.97, sd^{∞}, 50	sd-$^{\pi}\delta$: 1.96, $sd^{4.5}$, 50
W	+0.22	99.1	MH: 1.96, $sd^{1.9}$, 39	2.00, sd^{∞}, 50	d-δ: 2.00, sd^{∞}, 49
			MM: 2.00, $sd^{1.5}$, 50	1.97, sd^{∞}, 50	sd-$^{\pi}\delta$: 1.99, $sd^{2.9}$, 50

Table 8. NRT-Computed M−M Bond Orders for Group 6 HMMH Models along with Leading Resonance Configurations

M	MM bond order	VII	VIII	IX
Cr	4.64[a] (4.65,[b] 4.15,[c] 4.05[d])	55%[a] (55%,[b] 20%,[c] 12%[d])	29%[a] (29%,[b] 63%,[c] 69%[d])	12%[a] (12%,[b] 10%,[c] 13%[d])
Mo	4.58 (4.53[e])	53% (53%)	34% (34%)	8% (8%)
W	4.58 (4.55[f])	57% (57%)	37% (37%)	4% (4%)

[a] RDFT(B3LYP) computation at 1.64 Å Cr−Cr distance. [b] UDFT(B3LYP) broken-symmetry computation at 1.64 Å Cr−Cr distance. [c] UDFT(B3LYP) broken-symmetry computation at 1.83 Å Cr−Cr distance. [d] UDFT(BLYP) broken-symmetry computation at 1.83 Å Cr−Cr distance. [e] UDFT(BLYP) broken-symmetry computation at 1.94 Å Mo−Mo distance. [f] UDFT(BLYP) broken-symmetry computation at 2.23 Å W−W distance.

HMMH models, one might expect the resonance structures (**VII** and **VIII**) to make the greatest contributions. As summarized

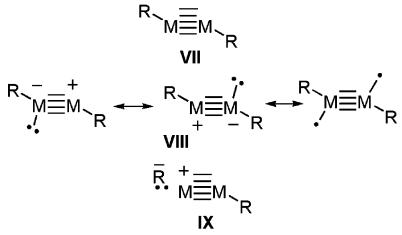

in Table 8, NRT analysis consistently exhibits bond order between four and five, thereby providing strong evidence for the characterization of the M−M bond as a *quintuple* bond. For both Mo and W compounds, the use of broken-symmetry computations has little affect on the bond orders or major resonance structures. The dimer, HCrCrH, is more complicated, as shown by the energy lowering upon breaking symmetry and the concomitant occurrence of significant spin contamination. At 1.83 Å Cr−Cr separation, similar to the experimental value for **1**, the NRT bond order barely exceeds four with either the B3LYP or BLYP functional. However, it must be kept in mind that, at this distance, the wave function is rather severely spin-contaminated ($S^2 = 2.1-3.2$). Large contributions from higher spin states, which are physically unrealistic given the distinctly diamagnetic character of the experimental compound, lower the overall computed bond order. Therefore, one can safely describe the "true" metal−metal bond order as being between four and five.

Rotation about the HM−MH Bond. The consequences of rotation about the HM−MH bond are consistent with quintuple bond character and the existence of an energetically substantial M−M "side-on d-bond" (sd-$^{\pi}\delta$). Variation of the HMMH torsion angle from 0° to 180°, while keeping the HMM angles fixed but allowing the HM and MM bond lengths to relax, creates nearly symmetrical energy profiles for Mo and W and a less symmetric profile for Cr (Figure 6). At approximately 35 kcal/mol, the barriers to rotation are large! To a first approximation, the M−M σ-bonds and the two M−M d-π-bonds should not change during rotation due to their cylindrical symmetry. Ignoring, for the moment, any hyperconjugative interactions, the M−H σ-bonds also should not be affected by rotation. In contrast, the pure M−M d-δ-bond overlap is sensitive to the torsion angle with C_4 symmetry (maxima at 0°, ±90°, and 180°). Strong directionality also characterizes the curious M−M "side-on d-bond" (sd-$^{\pi}\delta$) with C_2 torsional

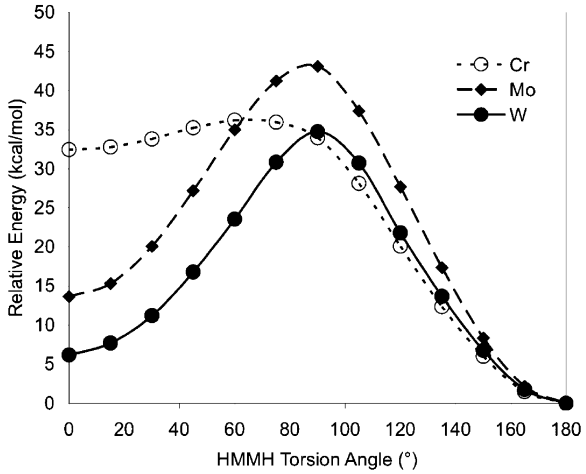

Figure 6. Energy surface for rotation of the transition metal HMMH central bond with fixed HMM bond angles as computed by the DFT(B3LYP) method. The M−M bond lengths increase upon rotating from 180° to 0° (Cr, 1.641 to 1.719 Å; Mo, 2.026 to 2.061 Å; W, 2.097 to 2.116 Å).

Table 9. Energy Differences (kcal/mol) between Bonding and Antibonding NBOs of Transition Metal Trans-Bent HMMH Molecules

NBO	Cr	Mo	W
M−M d-δ	83	69	69
M−M sd-$^{\pi}\delta$	122	132	103
M−M d-π	175	159	157
M−H sd-σ	261	261	268
M−M sd-σ	335	198	281

symmetry (maxima at 0° and 180°, minima at ±90°). Appearance of a large, single maximum at 90° is therefore consistent with M−M sd-$^{\pi}\delta$ interactions dominating the torsional surface. For Cr, the rotation surface is distinctly asymmetric, with the cis-bent structure nearly as high in energy as the 90° maximum. It appears that this behavior results from rather strong secondary interactions (such as hyperconjugation and H−Cr bond repulsions, both being enhanced by the extremely short (1.70 Å) Cr−Cr bonds and more polar Cr−H bonds) that modify the barrier profile expected from the idealized Lewis-like skeletal bonding.

Bond−Antibond Splittings. Relative strengths of σ-, π-, and δ-bonds are ordered by examination of the energy differences between the localized bonding and antibonding orbitals (Table 9). It is expected that these differences increase as the overall strength of the bonding interaction increases. A significant advantage of using localized orbitals rather than canonical molecular orbitals for this analysis is that interference due to mixing of ligand orbitals (in this case H) is removed. As the data in Table 9 reveal, the transition metal M−M bond "strengths" increase as d-δ < sd-$^{\pi}\delta$ < d-π < sd-σ. The lower stabilization afforded by the M−M d-δ-bond relative to the M−M side-on d-bond (sd-$^{\pi}\delta$) can be attributed to lower overlap in the former. Because the Group 6 M−M distance are so much shorter than those for the Group 14 analogues, the energy splittings tend overall to be larger, as expected when the π and δ overlaps become more consequential. For HWWH, rotation to the staggered position (90° torsion angle) significantly weakens the M−M side-on d-bond (sd-$^{\pi}\delta$) such that the bond−antibond splitting is lowered from 132 kcal/mol to just 39 kcal/mol, with little effect on the other orbital splittings. Thus, it is not surprising that the barriers to rotation about the M−M bonds are so large for the transition metals.

Table 10. Energies (kcal/mol) of Hydrogenation Reactions for Group 6 M−M Bonds According to $H_nMMH_n + H_2 \rightarrow H_{n+1}MMH_{n+1}$ (or MH_6)

M	$n=1$	$n=2$	$n=3$	$n=4$	$n=5$
Cr	−5.9	5.2	*a*	*a*	*a*
Mo	−19.8	−18.8	8.7	23.8[b]	23.8[b]
W	−38.9	−42.7	34.3	21.0[b]	21.0[b]

[a] Complexes with formulas H_4CrCrH_4, H_5CrCrH_5, and CrH_6 are unstable with respect to formation of molecular H_2 complexes or bridging hydrides. [b] H_5MMH_5 complexes are unstable with respect to molecular H_2 complex formation; values listed are one-half of the energies of hydrogenation for $H_4MMH_4 + 2H_2 \rightarrow 2\ MH_6$.

Heats of Hydrogenation. In contrast with the observation for unsaturated p-block molecules, the magnitude of absolute hydrogenation energies of unsaturated dinuclear transition metal species increases down the Group 6 column (Table 10). This pattern mirrors the well-established trend of increasing bond enthalpies down a column of transition metals. For transition metals, the strengths of M−H bonds are sufficiently weak that alternate bond topologies, such as molecular hydrogen complexes and bridging hydrides, commonly lie close in energy. Compositions such as H_mCrCrH_m (m = 4, 5, and 6) and H_5MMH_5 (M = Mo, W) are unstable as simple, terminal hydrides and optimize to true local minima containing H−H bonds or bridging H's. The exothermic hydrogenations of Mo and W M−M δ-bonds (n = 1 and 2) suggest weak M−M interactions relative to the M−H bonds. In contrast, hydrogenation of the M−M π- and σ-bonds (n = 3−5) is endothermic, indicative of the expected greater strength of M−M π-bonding compared to δ-bonding.

Origin of Linear vs Trans-Bent Structures. Adoption of linear geometries by HMMH molecules of the d-block requires significant electronic structure rearrangements. For the transition series, formal quintuple bond character is achieved through a combination of one σ-bond, two π-bonds, and two δ-bonds in the linear geometry. Unlike the trans bent structure, in the linear geometry the two δ-bonds are unhybridized (pure d AOs). Hybrids making the M−H and M−M σ-bonds in the linear geometry are symmetric and antisymmetric combinations of s- and d_{z^2}-orbitals. These combinations do not yield equivalent maximum strength hybrids. Whereas the M−H bond has the expected characteristics of a σ-bond with a strong concentration of electron density along the internuclear axis, orthogonality constraints force the M−M σ-bond to adopt an unusual "ringed σ-bond", as shown in Figure 7. This wave function places most of the density in a cylinder around the internuclear axis (the outer ring), with a smaller proportion of opposite phase located along the internuclear M−M axis (the inner ring); a cylindrical node separates the inner and outer rings. For such a "ringed σ-bond", we use the "sd-$^{\odot}\sigma$ " label, where the superscripted symbol evokes the electron density cross section at the midpoint of the M−M axis.

In the d-block, the M−M bond length decreases on moving from the trans-bent to the linear geometry, but the M−H bond length increases. We attribute this pattern to the compromised nature of the M−H and M−M σ-bonds, enforced by the linear geometry. The odd M−M ringed σ-bond (sd-$^{\odot}\sigma$) requires shortening to compensate for loss of overlap, whereas the M−H bond is lengthened due to higher s-character (50%) than the idealized hybridization (ca. 35% s-character). In the transition metal series, ns-orbitals have larger radii than the (n − 1)d-orbitals; as a result, more metal s-character tends to lengthen σ-bonds.

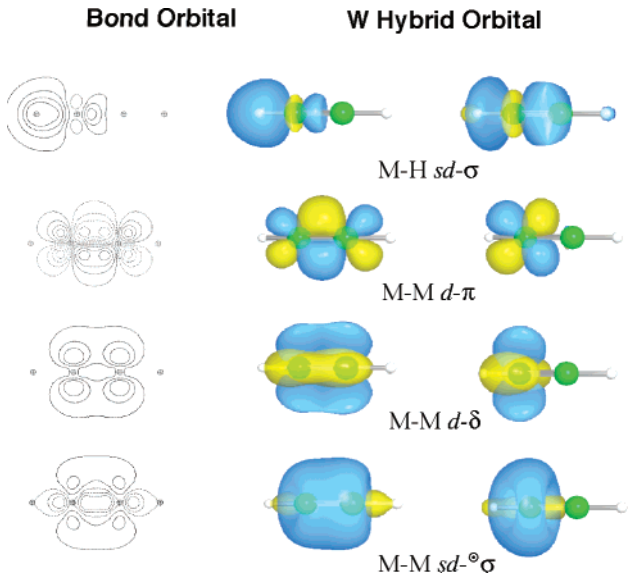

Figure 7. Natural bond orbitals (NBOs, left and center columns) and W-centered natural hybrid orbitals (NHOs, right column) for linear HWWH that describe M−H sd-σ-bond (top row), one of the two equivalent M−M d-π-bonds (second row), one of the two equivalent M−M d-δ-bonds (third row), and the M−M ringed σ-bond (sd-$^{\odot}\sigma$) (fourth row).

Why should Group 6 RMMR molecules adopt trans-bent geometries? As in the Group 14 series, the strong directed valency of the σ-bonding framework sets the stage for the rest of the electronic structure. For the transition metals, σ-bond stabilization favors substantial hybridization of the M valence s- and d-orbitals. For the Group 6 RMMR compounds, the attachment of two atoms to each M dictates approximately "sd^1" idealized σ-bonding hybrids. Due to the shapes of "sd^1" hybrids, HMM bond angles near 90° result and ultimately produce the trans-bent geometry. Maximization of the remaining valency leads to a bond order that is close to five, thereby providing strong support for the formulation of **1** as a quintuple bond.

Extensions to "Hypervalent" Metal Complexes. The quintuply bonded HCrCrH model with a 12e count at Cr is exceptional. Most transition metal compounds have formal electron counts greater than 12e because the Lewis-like parent structure is seldom protected from coordination of additional ligands that increase the formal electron counts. Exemplary of the more common higher coordination numbers and electron counts is the famous quadruply bonded, 16e $Re_2Cl_8^{2-}$ anion.[66] Indeed, even the Power complex, **1**, could be characterized as a 14e count due to weak donation from aryl rings. How does one accommodate increased electron counts and metal−metal multiple bonds within a localized bond framework based on metal s- and d-orbitals?

The centrosymmetric character of the sd^n metal hybrid orbitals, modest bond strengths, and prevailing polarities of M−X bonds make the corresponding M−X *antibonding* orbitals highly accessible acceptors for electron pair donors. For example, one might expect that the Cr−H antibonds of HCrCrH may serve as powerful acceptors for backside electron-pair donors, thus creating a three-center, four-electron (3c/4e)

(66) Cotton, F. A.; Curtis, N. F.; Harris, C. B.; Johnson, B. F. G.; Lippard, S. J.; Mague, J. T.; Robinson, W. R.; Wood, J. S. *Science* **1964**, *145*, 1305.

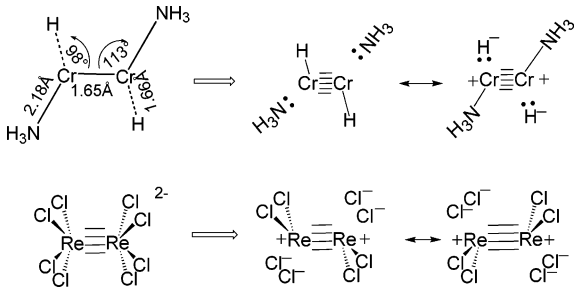

Figure 8. Structures and primary resonance configurations of (NH_3)-$HCrCrH(NH_3)$ and $Cl_4ReReCl_4^{2-}$.

bonding arrangement. Such a hypervalent bonding mode can be described by use of the resonating structures shown in Figure 8 for NH_3 as donor ligand. Donation of the N lone pair into the Cr−H antibond is maximized when the donor approaches from the back side (metal end) of the Cr−H bond. Indeed, DFT computations demonstrate such a geometry for $(NH_3)HCrCrH$-(NH_3) (Figure 8). The Cr−N interaction is weak, yielding a geometry-optimized bond length of 2.23 Å. Both the NCrCr and HCrCr bond angles open to values near 110°, apparently due to substantial donation of electron density into the Cr−Cr d-π^* antibonding orbital as well as the Cr−H antibonding (sd-σ^*) orbital.

The bonding of $Re_2Cl_8^{2-}$ can be constructed from the hypothetical $Re_2Cl_4^{2+}$, a fragment comprising 12e counts at each Re, a Re−Re quadruple bond, and sd^2 hybridization in the σ-bond framework (Figures 3 and 8). Addition of four Cl^- ligands, two per Re, backside to the Re−Cl bonds completes the structure. The overall square pyramidal coordination geometry at each Re center and the eclipsed conformation of the Re−Cl bonds are the natural consequences of two 3c/4e bonds per Re and a Re−Re quadruple bond. Similar considerations allow one to construct the bonding patterns of most metal−metal multiple bonds.

Summary

Much of the power of modern chemistry derives from the existence of simple models, such as Lewis structures, that summarize diverse and complex phenomena. Superficially, the trans-bent geometries exhibited by maximally bonded main group and transition metal complexes, such as **1** and **2**, seem strange because the structures belie expectations based on alkyne geometries. Nonetheless, simple application of Lewis-like structures and hybridization tendencies make such "strange" molecular shapes understandable. Throughout much of the periodic table, hybridization makes for stronger electron-pair σ-bonds. The extent to which bonding-active valence atomic orbitals mix to form hybrids depends most critically on the radial match of these orbitals and the polarity of the resulting bond (Bent's rule). Among the Group 14 elements, carbon valence s and p atomic orbitals have most similar radial extents and mix most extensively. As one proceeds down Group 14, the p-character in the σ-bonding hybrid orbitals increases. Extensive use of valence p AOs in making the stronger σ-bonds occurs at the expense of the weaker p-π-bonds; formation of two "normal" p-π-bonds is not possible, thereby resulting in a weak, slipped $(sp\text{-}^{//}\pi)$ bond in the molecular plane. Similar reasoning applies to Group 13 dianions, such as $[HGaGaH]^{2-}$.

For transition metals, the strongest σ-bonds result from mixing of metal valence ns- and $(n-1)$d-AOs to form sd hybrids. Hybridization is more effective in the second and third transition series than the first, because of the better match between radial distributions of the valence s and d AOs in the second and third series. Due to their strongly directional character, sd hybrids intrinsically favor nonlinear bond arrangements. For Group 6 RMMR dimers, there are enough valence orbitals to make two σ-bonds at each metal center and four additional, but weaker, M−M bonds: two π-bonds and two "δ-like" bonds. Thus, a quintuple M−M bond not only is reasonable but should be expected so long as amenable synthetic routes to sterically protected dimers can be devised, as in the spectacular synthesis of **1**. An interesting consequence of hybridization is that one of the two M−M "δ-like bonds" has distinct $\sim sd^4$ hybrid character and is stronger than the conventional M−M d-δ-bond. The Lewis-like model presented here is readily extended to more conventional metal dimers with multiple metal−metal bonds, such as $Cl_4ReReCl_4^{2-}$, by straightforward consideration of 3c/4e bonding interactions.

Based on the number of shared electron pairs that play a significant role in holding the M−M atoms together, there is ample justification for assignment of bond orders approaching three in Group 14 (for M = C, Si, Ge, Sn) and approaching five in Group 6 (M = Cr, Mo, W). For RMMR dimers of the transition metals, M−M quintuple bonding should be more robust, and less complicated by antiferromagnetic character, for M = Mo and W than for the recently synthesized Cr dimer.

Acknowledgment. We thank Professors Larry Dahl and Phil Power for inspiring discussions.

Note Added after ASAP Publication. After this paper was published ASAP on May 12, 2006, the Ge−Ge bond length in the drawing of chemical structure **2** was corrected. The corrected version was published ASAP on May 15, 2006.

Supporting Information Available: Cartesian coordinates and total energies for computed structures. This material is available free of charge via the Internet at http://pubs.acs.org.

JA060992U